Paper I

ELSEVIER

NeuroImage

www.elsevier.com/locate/ynimg
NeuroImage 29 (2006) 965 – 976

NG2 expression regulates vascular morphology and function in human brain tumours

C. Brekke,[a] A. Lundervold,[a] P.Ø. Enger,[a] C. Brekken,[b] E. Stålsett,[a] T.B. Pedersen,[b] O. Haraldseth,[b,c] P.G. Krüger,[a] R. Bjerkvig,[a,d] and M. Chekenya [a,*]

[a]*Department of Biomedicine, Section for Anatomy and cell biology, University of Bergen Jonas Lies Vei 91, N-5009 Bergen, Norway*
[b]*Fuge Molecular Imaging Center, Department of Circulation and Medical Imaging, Norwegian University of Science and Technology, N-7465 Trondheim, Norway*
[c]*Department of Medical Imaging, St. Olavs Hospital, Trondheim, Norway*
[d]*Norlux, Neuro-Oncology, Centre Recherche Public de la Santé, Luxembourg, Belgium*

Received 12 May 2005; revised 18 July 2005; accepted 23 August 2005
Available online 25 October 2005

Tumour angiogenesis is a tightly regulated process involving cross-talk between tumour cells and the host tissue. The underlying mechanisms that regulate such interactions remain largely unknown. NG2 is a transmembrane proteoglycan whose presence on transformed cells has been demonstrated to increase proliferation in vitro and angiogenesis in vivo. To study the effects of NG2 during tumour growth and progression, we engineered an NG2 positive human glioma cell line (U251-NG2) from parental NG2 negative cells (U251-WT) and implanted both cell types stereotactically into immunodeficient nude rat brains. The tumours were longitudinally monitored in vivo using multispectral MRI employing two differently sized contrast agents (Gd-DTPA-BMA and Gadomer) to assess vascular leakiness, vasogenic oedema, tumour volumes and necrosis. Comparisons of Gd-DTPA-BMA and Gadomer revealed differences in their spatial distribution in the U251-NG2 and U251-WT tumours. The U251-NG2 tumours exhibited a higher leakiness of the larger molecular weight Gadomer and displayed a stronger vasogenic oedema (69.9 ± 15.2, $P = 0.018$, compared to the controls (10.7 ± 7.7). Moreover, immunohistochemistry and electron microscopy revealed that the U251-NG2 tumours had a higher microvascular density (11.81 ± 0.54; $P = 0.0010$) compared to controls (5.76 ± 0.87), with vessels that displayed larger gaps between the endothelial cells. Thus, tumour cells can regulate both the function and structure of the host-derived tumour vasculature through NG2 expression, suggesting a role for NG2 in the cross-talk between tumour–host compartments.

Keywords: Angiogenesis; Multispectral MRI; Gadomer; Glioblastoma; NG2

Introduction

A basic concept in tumour biology is that neoplastic growth depends on angiogenesis (Folkman, 1995). Glioblastoma Multiforme (GBM), the most common and anaplastic brain tumour in adults, is characterised by florid angiogenesis, increased vascular permeability and focal necrosis (Burger and Kleihues, 1989). Human GBMs are further denoted by diffuse infiltration of tumour cells into the brain parenchyma, where they are initially supported by the pre-existing vasculature through the process of vessel co-option (Holash et al., 1999). Later, as the tumour grows beyond a size rate limited by oxygen and nutrient diffusion, a switch in the balance between inhibitors and stimulators triggers angiogenesis (Folkman et al., 1971). Although the formation of new vessels is a constant finding in all solid tumours, animal experiments have demonstrated that different cancer cell lines implanted at the same site recruit vessels with different microvascular architecture (McDonald and Choyke, 2003). Although these cell lines do not disseminate diffusely into the brain, they are useful in studying angiogenesis in animal models. For example, early studies showed high correlation between angiogenic GBM tumours in vivo and potent angiogenic factors secreted by GBM cell lines in vitro (Klagsbrun et al., 1976). Others have shown that conditioned medium from either GBM tumour explants or established cell lines, contained potent and specific endothelial cell mitogens in vitro and in vivo, and that almost all malignant glioma cell lines express epidermal growth factor receptor (EGFr), of which the majority of GBM tumours have gene amplification or rearrangement (Sang et al., 1989). So, the angiogenesis observed in experimental studies using cell lines xenografted into nude rat brains may be highly informative of the complex communication networks between the tumour–host microenvironment during vascular formation in cancer patients. The exact mechanisms that regulate such networks are still poorly described. Since tumour angiogenesis coincides with poor prognosis, specific mechanisms that regulate vascular morphology may represent novel targets for therapy.

NG2 is a transmembrane proteoglycan that correlates with an aggressive disease course when expressed on tumour cells. It

* Corresponding author.
E-mail address: Martha.Chekenya@iac.uib.no (M. Chekenya).
Available online on ScienceDirect (www.sciencedirect.com).

1053-8119/$ - see front matter © 2005 Elsevier Inc. All rights reserved.
doi:10.1016/j.neuroimage.2005.08.026

increases tumour cell proliferation in vitro and promotes angiogenesis in vivo that predisposes animals to poorer survival outcomes by binding angiostatin (Chekenya et al., 2002b; Goretzki et al., 2000). We have previously reported NG2 expression in 13/18 human glioblastomas from patient biopsy material (Chekenya et al., 2002a). NG2 was expressed on both the tumour cells and their associated vasculature. Vessel associated NG2 was localised on both the pericyte and basement membrane components of the tumour vasculature. NG2 is also widely expressed on newly formed blood vessels during wound healing where its expression is restricted to "activated" microvascular pericytes (Ozerdem and Stallcup, 2003; Schlingemann et al., 1990). Pericytes are present at very early stages of angiogenesis, and are thought to stimulate endothelial cell recruitment and guide the formation of capillary tubes via cell–cell interactions or through the release of soluble factors (Fukushi et al., 2004; Nehls et al., 1992; Ozerdem et al., 2001, 2002; Schlingemann et al., 1990). Whether the vessels in NG2 expressing tumours are functionally different from those associated with NG2 negative tumour cells is not known. To address this issue, we used serial MRI and implemented pharmacokinetic models and multispectral data analysis to compare fundamental tumour characteristics such as vascular volume, permeability, tumour growth, peritumoural oedema and necrosis in the NG2 expressing U251 tumours (U251-NG2) and the wild type U251N human GBM tumours (U251-WT) xenografted into immunodeficient nude rat brains over time. Increased permeability is a uniform finding in tumour vasculature which gives rise to increased leakage of contrast agents. Dynamic contrast-enhanced (DCE) MRI, primarily with small-molecular-weight contrast agents (gadolinium diethylenetriamine penta-acetic acid bismethylamide; Gd-DTPA-BMA), has been extensively used to diagnose tumours and to monitor microvascular parameters. However, whilst Gd-DTPA-BMA is useful in distinguishing defective and leaky tumour endothelium from the normal counterparts, it only marginally discriminates the vasculature of distinct tumour types (Daldrup et al., 1998; Su et al., 1998). Therefore, we also used the high-molecular-weight dendritic tracer Gadomer in DCE MRI for the assessment of vascular permeability and blood volumes. We also compared the spatial distribution of Gd-DTPA-BMA and Gadomer in tumour tissue to distinguish between vasculatures of different leakiness. Furthermore, we correlated the MRI data analysis of microvascular parameters as well as tumour growth, vasogenic oedema and necrosis with histological and ultra structural analyses of the tumours. The present findings demonstrate that the tumour vasculature in U251-NG2 tumours is structurally and functionally different from that in U251-WT tumours, suggesting that NG2 expressed by tumour cells may modulate vessel structure during tumour angiogenesis. Since these alterations in microvascular architecture also were accompanied by a more aggressive disease course, NG2 may represent a target for future therapies.

Methods

Cell culture

The human glioblastoma (GBM) cell line U251N (American Type Culture Collection, Rockville, MD) was transfected with the NG2 cDNA as previously described (Chekenya et al., 2002b). The cells were propagated in Dulbecco's Modified Eagle's (DMEM) medium supplemented with geneticin disulphate (800 g/ml) (Sigma, Dorset, United Kingdom) as described previously (Chekenya et al., 2002b). Multicellular spheroids were made by seeding 3×10^6 cells in 10 ml DMEM into 75 cm^2 flasks base coated with agar as earlier described (Yuhas et al., 1977).

Animals

Nineteen, 6–7 week old immunodeficient nude rats (Han: rnu/rnu Rowett Nude), weighing approximately 30 g, of both sexes were bred in an isolation facility at 25°C (55% relative humidity) in a specific pathogen free environment and animal husbandry protocols were maintained as previously described (Chekenya et al., 2002b). Both sexes were used in order to rule out hormonal effects on tumour growth. In accordance with ethical guidelines, this enabled us to reduce the total number of animals bred for the experiments. All animal procedures were performed in accordance with protocols approved by The National Animal Research Authority (Oslo, Norway). The maximum follow-up time was 82 days for both groups (n = 10, U251-NG2 and n = 9, U251-WT).

Intracranial implantation

The animals were anaesthetised before surgical procedures with subcutaneous injections of fentanyl/fluamisone/midazolam as previously described (Thorsen et al., 2003). The rats were immobilised in a sterotaxic frame (David Kopf Instruments model 900, Tujunga, CA) and a burr hole was made 1.5 mm to the right of the sagittal suture and 0.5 mm posterior to the Bregma. 10 μl of phosphate buffered saline (PBS) containing 15 spheroids was injected into the forebrain to a depth of 1.5 mm from the brain surface. Closure was effected with 3.0 ethilon suture. The animals were sacrificed by CO_2 inhalation and decapitation when neurological signs became evident. The brains were then removed and fixed in 4% paraformaldehyde (PFA).

Histological and immunohistochemical evaluations

After fixation, the tumours were coronally cut in half exactly and the two blocks were processed separately for paraffin-wax embedding following standard procedures. With the cut edge facing the microtome, 5 μm thick tissue sections were cut in planes corresponding to those utilised in the MRI evaluations, and placed on poly-L-lysine coated glass slides. Tissue for histopathological examination was stained with Harris Haematoxylin and Eosin (H&E; Merck, Darmstadt, Germany) and examined with a Nikon Eclipse (E600) light microscope. Images were captured with a Nikon DXM1200 digital camera (Nikon Corporation, Tokyo, Japan). Indirect immunohistochemistry was performed using the EnVisionSystem, horse-radish peroxidase (HRP) and 3′3′-diaminobenzidine (DAB) (Dako, Glostrup, Denmark) method, as described in the manufacturer's protocol. Primary antibodies used to label formalin fixed, paraffin embedded tissue were: rabbit anti-human von Willebrandt Factor (vWF, diluted 1/500 in TBS; Dako), anti-human Vimentin (diluted 1/500 in TBS, Dako), rabbit anti-rat NG2 (diluted 1/500 in TBS), which was a generous gift from W.B. Stallcup, The Burnham Institute, San Diego, CA. Epitope retrieval was performed with Proteinase K (Dako) for vWF and citrate buffer (pH 6.5) for NG2 and Vimentin. Tissue sections immunostained using DAB and Fast Red were visualised and analysed using the image analysis system LUCIA, version 4.21 (Laboratory Imaging Ltd., Prague, The Check Republic). For immunocyto-

chemistry, glioma cells grown as monolayers were fixed in ice-cold 4% PFA for 10 min, prior to incubation with rabbit anti-rat NG2 antibodies (diluted 1:1000 in PBS) and Fluoro-isothiocynate (FITC) conjugated anti-rabbit secondary antibodies (ZYMED, San Francisco, CA) (diluted 1:100 in PBS) as described previously (Chekenya et al., 2002b). A Leica TCS NT confocal laser-scanning microscope (Leica Lasertechnik, Heidelberg, Germany) was used to visualise the specimens. U251-NG2 and U251-WT tumours immunostained for vWF or Ki67 were screened for areas with vascular hot spots or proliferating cells at ×40 low magnification. In each tumour (U251-NG2: $n = 3$; U251-WT: $n = 3$) for vWF or Ki67, 5 regions were selected for microvessel density (MVD) and microvessel area fraction (MVA) quantification using ×400 magnification, and the image analysis LUCIA system.

Transmission electron microscopy

For ultrastructural evaluations, one rat from each group was perfusion fixed using 2% glutaraldehyde in 0.1 M cacodylate buffer with 0.2 M sucrose (pH 7.2; 300 ± 10 mOsm) for at least 1 h via a cannula inserted in the left carotid vein. The brains were then removed and placed in the same fixative for 2 days. The tumours were then cut into 2 mm sized pieces and post-fixed for 1 h in 1% osmium tetroxide (OsO_4), dehydrated in graded ethanol concentrations and embedded in epon 812-propyleneoxide (Fluca, Buchs, Switzerland). The final polymerisation was carried out at 60°C for 24 h and thereafter semi-thin sections were stained with toluidine blue. The appropriate ultra-thin sections with relevant regions of interest were cut on a Reichert Ultracut Microtome (Leica Microsystems, Bensheim, Germany) stained with uranyl acetate and lead citrate and examined by a Jeol JEM-1230 transmission electron microscope (Jeol, Tokyo, Japan).

Magnetic resonance imaging

Only animals with a brain tumour and a successful MRI scanning at two different time-points were included in the MR image analyses, $n = 8$ in the U251-NG2 group and $n = 4$ in the U251-WT group. All animals included in the data analyses underwent repetitive MR scanning at 5 and 7 weeks after tumour implantation. MRI was performed on a 2.35 T Bruker Biospec Advance DBX-100 horizontal bore magnet (Bruker, Ettlingen, Germany), using a saddle-shaped RF coil with an inner diameter of 4 cm. The animals were continuously anaesthetised with 1–2% isoflurane in 70/30% N_2/O_2 through a facemask. The imaging order and the key parameters of the nine different 2 D pulse sequences are listed below, see also Table 1. The T2-weighted RARE (rapid acquisition with relaxation enhancement) sequence had the following imaging parameters: field of view (FOV) = 3 cm, repetition time (TR) = 6000 ms, echo time (TE) = 60 ms (effective), acquisition matrix 128 × 128, number of excitations (NEX) = 4, turbo factor = 8, slice thickness 1 mm (interslice distance 1.2 mm) and 11 axial slices. FOV/TR/TE/matrix/NEX for the T2-weighted fluid-attenuated inversion recovery (FLAIR) sequence were 3 cm/2500 ms/60 ms, 128 × 128/2, and with the same number of slices, slice thickness and interslice distance as the RARE sequence. T1-maps were calculated from five spin echo (SE) images with fixed TE and consecutive repetition times and used for calculation of the plasma concentration of the tracer (i.e. TR = 2000, 1500, 500, 300, 100 ms) with FOV/TE/matrix of 3 cm/8.8 ms/64 × 64, slice thickness 3 mm (interslice distance 3.5 mm) and 3 slices positioned to cover the central parts of the tumour. Enhancement kinetics and assessment of microvascular parameters were studied using a DCE imaging sequence with identical sequence geometry as used in the T1-maps. Contrast agents were infused through a polyethylene catheter inserted into one femoral vein at each examination. For DCE imaging, a bolus injection of 0.2 mmol/kg Gadomer (kindly provided by Dr. Berndt Misselwitz, Schering AG, Berlin, Germany) was administered after acquiring four baseline (pre-contrast) images, followed by a continuous set of 63 contrast-enhanced images (frames) with a temporal resolution of 16.7 s for the first 30 frames, which was increased to 43 s for the remaining frames, giving a total acquisition time of 32 min. Gadomer is a dendritic gadolinium chelate containing 24 Gd ions with a molecular weight of 17 kDa but because of its globular configuration, it has an apparent molecular weight of 30–35 kDa (Misselwitz et al., 2001). The DCE sequence was followed by a bolus injection of 0.5 mmol/kg Gd-DTPA-BMA (Omniscan®, Amersham Health, Oslo, Norway), which has a molecular weight of 0.58 kDa. After 2 min delay, a post-contrast SE T1-weighted imaging sequence was acquired (FOV/TR/TE/matrix/NEX = 3 cm/407 ms/13 ms/256 × 256/4). The slice positions in each sequence were the same so that subsequent multispectral analyses would be valid. The same imaging protocol was used at both imaging time-points, see also Fig. 1.

Pharmacokinetic models and multispectral MR analyses

The dynamic MRI data collected as signal intensities (SI) were converted to contrast agent concentration based on the

Table 1
The imaging sequences included in the protocol

Sequence	FOV [cm]	TR/TE [ms]	Acquisition matrix	NEX	Turbo factor	Slice thickness [mm]	No. of slices
T2 (RARE)	3	6000/60	128 × 128	4	8	1 (1.2)	11
FLAIR	3	2500/60	128 × 128	2		1 (1.2)	11
T1	3	2000/8.8	64 × 64			3 (3.5)	3
T1	3	1500/8.8	64 × 64			3 (3.5)	3
T1	3	500/8.8	64 × 64			3 (3.5)	3
T1	3	300/8.8	64 × 64			3 (3.5)	3
T1	3	100/8.8	64 × 64			3 (3.5)	3
DCE	3	122.5/5	64 × 64			3 (3.5)	3
Post-Gd-DTPA-BMA T1	3	407/13	256 × 256	4		1 (1.2)	11

T1-maps were created from five T1-images with consecutive TR times. The interslice distance is shown in brackets.

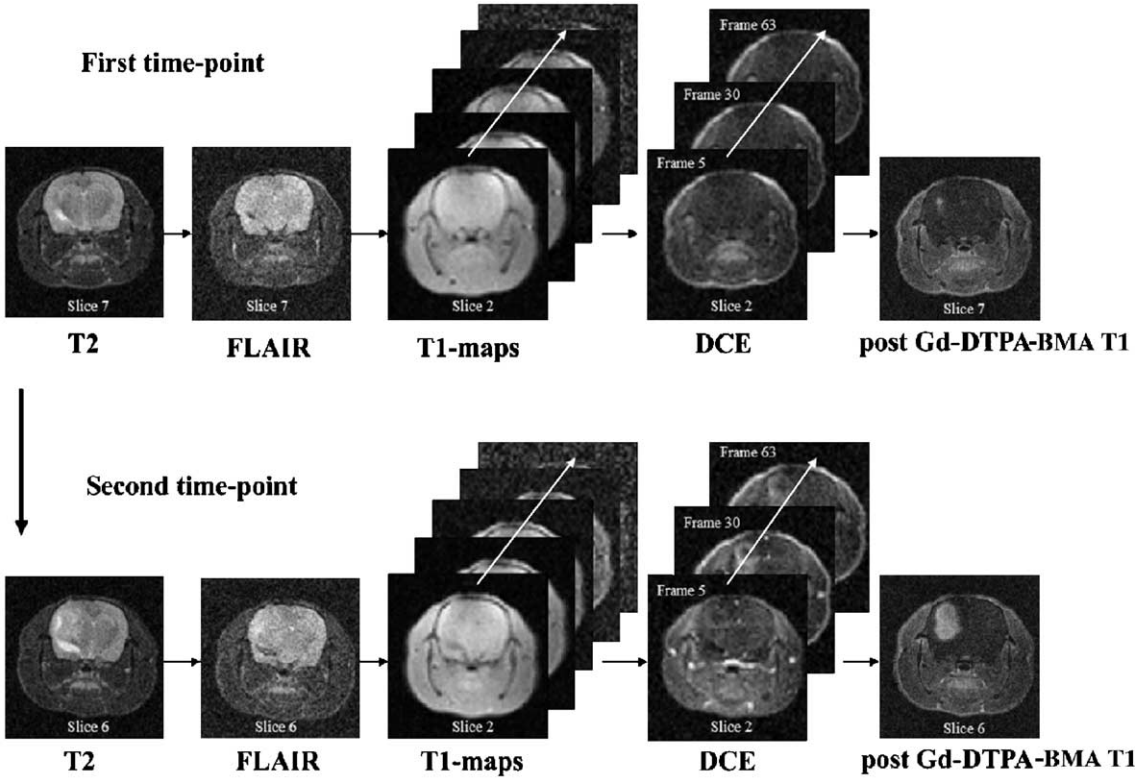

Fig. 1. Schematic diagram of the image acquisition timing. The figure shows the images acquired from the same animal at two time-points (i.e. 5 and 7 weeks) after tumour implantation.

general assumption that the increase in T_1 relaxation rate is proportional to the total tissue concentration (C_T) of Gd-based tracer as previously described (Donahue et al., 1997). Microvascular parameters were assessed using two different pharmacokinetic models in order to evaluate whether our results were biologically dependent or model-dependent. The dynamic MRI data were analysed using the model developed by Su et al. (1994) and the model developed by Tofts et al. (Tofts and Kermode, 1991; Tofts, 1997; Tofts et al., 1999). In Su's model, the time course of the calculated C_T can be described by the microvascular parameters fractional blood volume, D_0 [mM], which is related to the local blood volume, and D_1 [mM min^{-1}] which expresses the permeability or leakage from blood vessels to tissue. Finally, $C_T(t)$ is also determined by K_2 [min^{-1}], which expresses the elimination of tracer from tissue back to blood. In Toft's model, the contribution of tracer in the plasma to the total tissue concentration is neglected and fractional blood volume is therefore not calculated. Here, permeability is defined as K^{trans} [min^{-1}], which is dependent on vessel permeability and vessel surface. The elimination rate or wash-out of tracer from the tissue is defined as $k_{ep} = K^{trans} / v_e$ [min^{-1}], where v_e is the extravascular extracellular space (EES).

All image processing and analyses were performed in Matlab, v. 6.5 (Mathworks, Inc, Natick, MA). The images from all channels were re-sampled to a 256 × 256 matrix using bi-cubic interpolation without any filtering of the images. Regions of interest (ROIs) for computation of permeability parameters for individual animals were drawn a priori on an image from the DCE-sequence, using a frame with maximum signal enhancement and a slice covering the centre of the tumour. Voxels with delayed or no low contrast enhancement were excluded from the ROI, and the microvascular parameters were estimated on a pixel-by-pixel basis and parametric maps were generated. Solid tumour tissue, peritumoural oedema and necrosis were manually delineated and volumes estimated using colour encoded (RGB) multispectral images computed from geometrically corresponding post-Gd-DTPA-BMA T1-weigted, T2-weighted and FLAIR images. The amount of red in the RGB image was proportional to the SI in the T2-channel, and the amounts of green and blue were proportional to the SI in the FLAIR and post-Gd-DTPA-BMA T1-channel, respectively. Thus, voxels with high SI in more than one channel got a mixed colour. The volume of interest in each slice was then calculated as the number of pixels within a ROI determined by the colour encoding and multiplied with the voxel size of 0.0244 mm^3 (corrected for interslice gap). Three-dimensional scatter plots derived from the multispectral images were generated to show the different features of the tumour correlated to the SI in the three channels, where blue pixels represent solid tumour tissue, red pixels oedema, green pixels CSF, and black pixels necrotic tissue. The scatter plots were also used as a control for the delineation of the different tumour characteristics in the image. The tumour volume doubling (Vd) time for each group was determined as Vd = $t \cdot \log 2 / \log(V2 / V1)$ (Nakajima et al., 1998), from multispectral RGB images at each time-point, where, t is the time between each scanning, V2 and V1 are the solid tumour mean volumes for each group at the second time-point and at the first time-point, respectively. Colour encoded images generated from a post-Gd-DTPA-BMA T1-weigted image (encoded red) and a single frame from the DCE sequence (encoded green) were used for visualisation of spatial contrast enhancing patterns obtained with Gd-

DTPA-BMA and Gadomer, respectively. Images from the two channels used for comparison of contrast enhancement pattern represented corresponding slices and time-points after injection of the contrast agents.

Statistical analysis

Image data were analysed by non-parametric Mann–Whitney *U* tests using Graphpad Instat software version 3.05 (Graphpad Inc, San Diego, CA). The Kaplan–Meier (Kaplan and Meier, 1959) method and the log-rank test (Mantel and Haenszel, 1959) were used to generate and analyse survival curves.

Results

NG2 regulates vascular morphology

NG2 expressing tumours, U251-NG2, and the NG2 negative controls, U251-WT, were examined histologically to assess NG2's

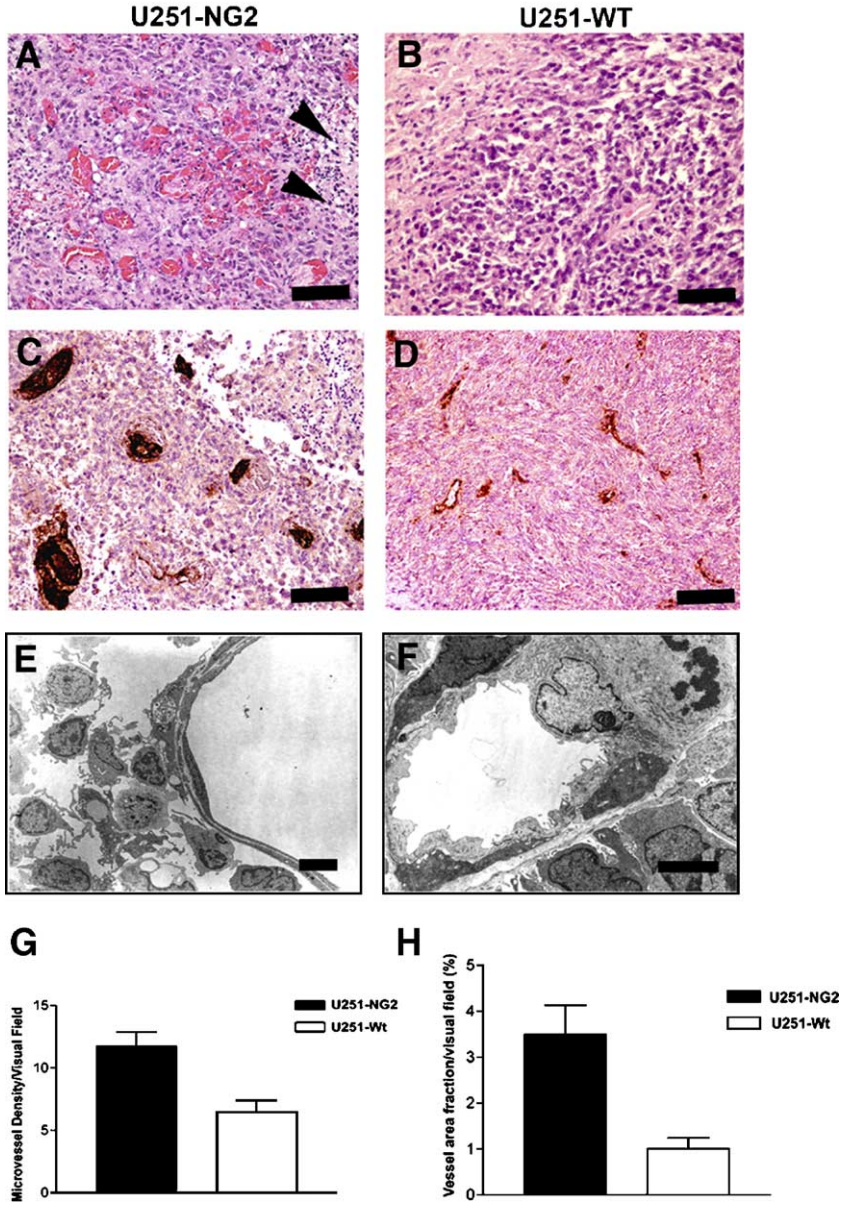

Fig. 2. NG2 regulates vascular morphology. (A) H&E stained histological section of a highly vascular U251-NG2 tumour showing stagnant blood lakes, necrosis with picnotic nuclei (black arrowheads), magnification 200×, scale bar 60 μm. (B) Histological section of U251-WT tumour showing less blood vessels and little necrosis, magnification 200×, scale bar 60 μm. vWF immunostaining of U251-NG2 (C) and U251-WT (D) tumour showing a highly abnormal vasculature in the U251-NG2 compared to the U251-WT tumours, magnification 200×, scale bar 60 μm. (E) Transmission electron microscopic image of U251-NG2 tumour showing large, dilated thin-walled vessels lacking pericyte coverage, magnification 1500×, scale bar 10 μm. (F) Transmission electron microscopic image of a U251-WT tumour showing small capillary-like vessels with distinct basement membranes and pericyte coverage, magnification 2200×, scale bar 10 μm. (G) Higher mean ± SEM MVD counts of vWF positive endothelial cells in U251-NG2 compared to U251-WT tumours, Mann–Whitney *U* test, $P = 0.001$. (H) Higher mean ± SEM MVA in the U251-NG2 compared to the U251-WT tumours, Mann–Whitney *U* test, $P = 0.001$. Quantified as described in Methods.

Table 2
Estimated microvascular parameters of U251-NG2 and U251-WT tumours

Vascular parameter	U251-NG2 5 weeks (n = 8)	U251-NG2 7 weeks (n = 8)	U251-WT 7 weeks (n = 4)
D_0 [mM]	0.0288 (0.0015)	0.0338 (0.0019)	0.0238 (0.0015), [a]P = 0.0121
D_1 [mM min^{-1}]	0.0560 (0.0043)	0.0628 (0.0019)	0.0488 (0.0019), [a]P = 0.0061
K_2 [min^{-1}]	0.1432 (0.0021)	0.0505 (0.0011)	0.0572 (0.0009), [a]P = 0.163
K^{trans} [min^{-1}]	0.0076 (0.0008)	0.0085 (0.0009)	0.0059 (0.0007), [a]P = 0.006
k_{ep} [min^{-1}]	0.0936 (0.0017)	0.0483 (0.0015)	0.0560 (0.0057), [a]P = 0.527

D_0 represents fractional blood volume, D_1 and K_2 express blood–tissue permeability and elimination rate, respectively, using Su's model. With Tofts' model, K^{trans} expresses blood–tissue permeability and k_{ep} the elimination rate of tracer from tissue. The results are expressed as means (±SEM). Results were considered statistically significant at $P < 0.05$ using Mann–Whitney U test.
[a] Compared to U251-NG2 tumours at 7 weeks.

role during tumour vessel formation. This comparison showed that NG2 expression caused a dramatic change in the tumour microvascular architecture as the vascular elements became both more numerous and structurally deranged. U251-NG2 tumours contained large areas with vascular "lakes" composed of tightly packed erythrocytes within dilated thin-walled vessels, Figs. 2A and E. In contrast, the U251-WT tumours exhibited a more homogeneous histological architecture with small, tightly packed tumour cells. The tumour core appeared hypovascularised and the endothelial cells were mostly associated with basement membranes (Figs. 2B and F). Immunolabelling for the vascular marker vWF displayed irregular and markedly dilated vessels in the U251-NG2 tumours with numerous endothelial cell proliferations, Fig. 2C. The vessels in the U251-WT tumours were smaller and less dilated, Fig. 2D. Ultrastructural examination of the NG2 tumours revealed abnormally thin-walled vessels with flat nucleated endothelial cells that resembled embryonic post-capillary venules, Fig. 2E. There were no obvious gap junctions and the basement membrane was very thin and disordered. There were areas of variable extension lacking pericyte coverage. These features were in striking contrast to the endothelium of the U251-WT tumours, which exhibited thicker blood vessels with a more regular endothelial lining, Fig. 2F.

The microvascular density (MVD) and the area fraction representing vascular elements (MVA) were estimated using computer-assisted imaging analysis. Quantification of MVD

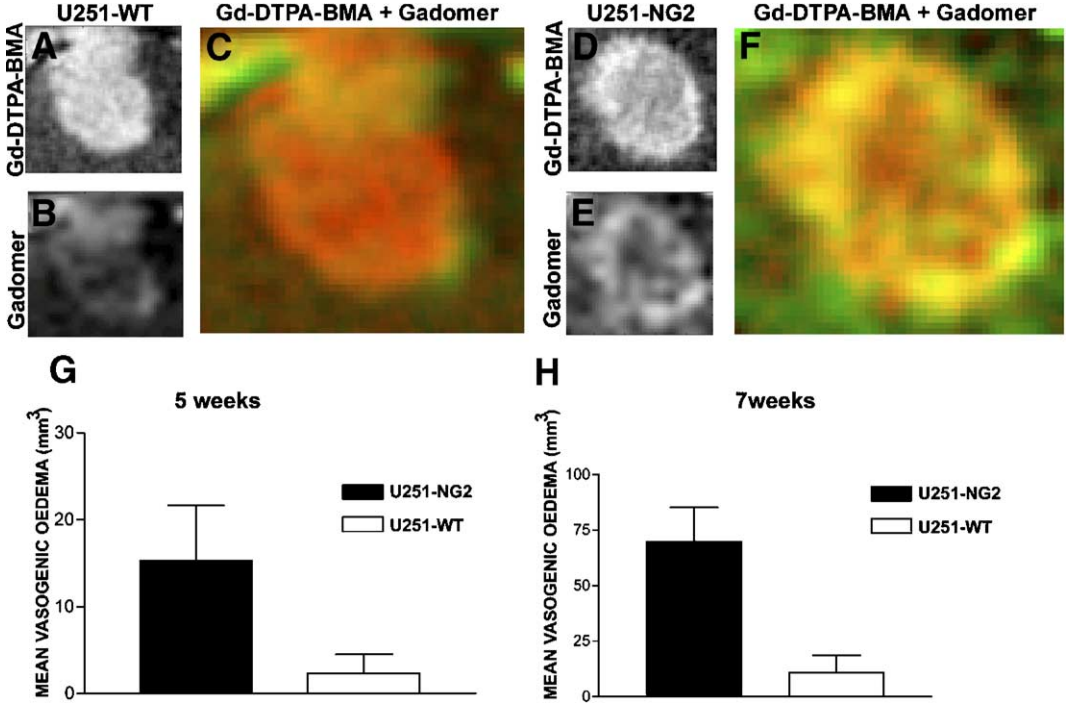

Fig. 3. NG2 regulates vascular function. In panel A, post-Gd-DTPA-BMA T1-weighted image showing high and homogeneous gadolinium contrast enhancement throughout the U251-WT tumour. (B) A temporally and geometrically corresponding image from the DCE sequence of U251-WT tumour showing low Gadomer contrast enhancement in the tumour rim and no enhancement centrally in the tumour. (C) Computed colour encoded images where Gd-DTPA-BMA (red) and Gadomer (green) indicating higher leakage of small-molecular-weight contrast agent Gd-DTPA-BMA, seen as a predominance of the red colour in the RGB image. (D) Post-Gd-DTPA-BMA T1-weighted image showing high gadolinium contrast enhancement throughout the U251-NG2 tumour. (E) DCE image of U251-NG2 tumour showing high Gadomer contrast enhancement peripherally in tumour. (F) Colour encoded image where Gd-DTPA-BMA (red) and Gadomer (green) indicate high leakage of both Gd-DTPA-BMA and Gadomer contrast agents peripherally (seen as yellow in RGB image). Central parts of the tumour show a higher vessel leakiness of small molecular substances (seen as orange in RGB image). Higher vasogenic oedema in U251-NG2 tumour bearing animals compared to U251-WT controls at (G) 5 week time-point, Mann–Whitney U test, P = 0.040 and (H) 7 weeks time-point, Mann–Whitney U test, P = 0.018.

counts of vWF stained tissue sections revealed higher vessel counts in the U251-NG2 tumours compared to the U251-WT controls, Fig. 2G, Mann–Whitney U test, $P = 0.0010$. Similarly, the microvascular area was significantly higher in the U251-NG2 compared to the U251-WT tumours, Fig. 2H, Mann–Whitney U test, $P = 0.001$. These MVD and MVA counts are consistent with those obtained using other passaged tumours in nude rat brains (data not shown).

NG2 regulates vascular function

To clarify whether these alterations in vascular morphology were also accompanied by functional changes, we estimated microvascular parameters such as permeability, blood volume and elimination rate of tracer. There was an increase in blood–tissue permeability (D_1, K^{trans}) and fractional blood volume (D_0) between the two time-points (i.e. 5 and 7 weeks) in the U251-NG2 tumours (see Table 2). However, we found a decreased wash-out of tracer from tumour tissue in NG2 expressing tumours at the second time-point compared to 5 weeks. Analyses of longitudinal microvascular changes in the U251-WT tumours were not performed due to the small tumour volumes at 5 weeks. There was higher vessel leakiness ($P = 0.006$) and fractional blood volume ($P = 0.0121$) in U251-NG2 compared to U251-WT tumours at 7 weeks. In contrast, there was no significant difference in the contrast elimination rates (K_2, k_{ep}), between the U251-WT and U251-NG2 tumours, $P = 0.163$ and $P = 0.527$, respectively (Table 2). The differences in blood fraction and blood–tissue permeability also persisted when comparing tumours of similar sizes, but here, U251-NG2 tumours revealed a higher elimination rate of tracer from tumour tissue than the U251-WT tumours.

Comparison of contrast enhancement patterns using two contrast agents with different molecular weights (i.e. Gd-DTPA-BMA and Gadomer) revealed differences in their spatial distribution in U251-NG2 and U251-WT tumours of the same size. Both tumours had a more clearly delineated edge with Gd-DTPA-BMA, Figs. 3A and D. Larger regions within the solid tumour tissue in the parental tumours had little or no enhancement with Gadomer, Fig. 3B, and colour encoded images revealed more prominent Gd-DTPA-BMA permeability compared to Gadomer in U251-WT tumours, indicated by the predominance of the red channel, Fig. 3C. In contrast, U251-NG2 tumours revealed both high ring enhancement with Gd-GTPA, Fig. 3D, and larger regions within the solid tumour tissue with Gadomer contrast enhancement, Fig.

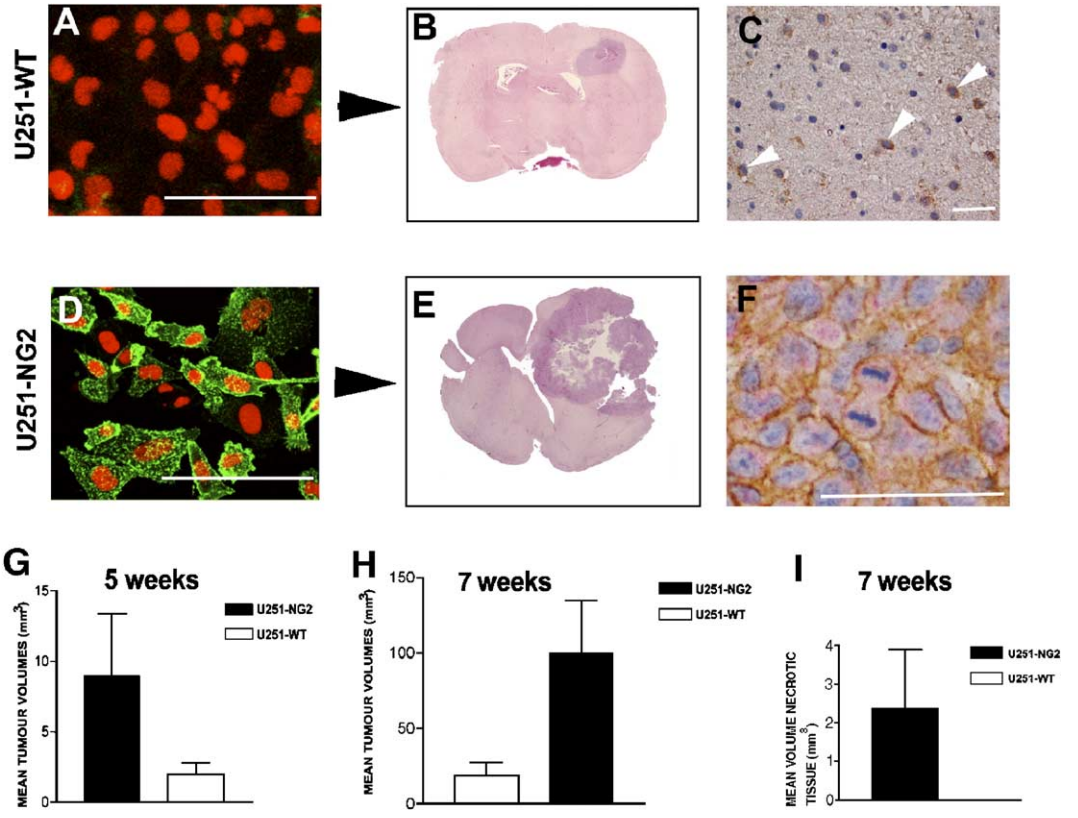

Fig. 4. NG2 expression increases tumour growth. Indirect immunocytochemical staining for NG2 (green) in U251-WT (A) and U251-NG2 cells (D). Propidium iodide (red) was used as nuclear counterstain, magnification 630×, scale bar 60 μm. Composite H&E stained histological section from an entire rat brain showing a homogenous small U251-WT tumour (B) and a large highly necrotic U251-NG2 tumour (E), magnification 40×. (C) Immunohistochemical staining shows that NG2 is expressed only on oligodendrocyte precursor-like cells in the normal brain of U251-WT tumour bearing animals (white arrowheads, magnification 100×, scale bar 50 μm) (F) Double immunohistochemistry for NG2 (DAB, brown) and pan-human vimentin (Fast Red), showing that the tumour cells are of human origin and express NG2 in U251-NG2 tumours. Mitotic figures are seen. Haematoxylin nuclear counterstain (blue), magnification 200×, scale bar 60 μm. High volumes of U251-NG2 tumours compared to U251-WT determined by MRI at 5 weeks time-point (G), but not statistically significantly different, Mann–Whitney U test, $P = 0.065$. (H) Significant difference between U251-NG2 and U251-WT tumour volumes at 7 weeks, Mann–Whitney U test, $P = 0.019$. (I) Necrosis was not present in the U251-WT tumours and was only apparent in U251-NG2 tumours after 7 weeks. Data represent MRI determined mean volumes ± SEM [mm^3].

3E. The multichannel colour encoded images also indicated that the U251-NG2 tumours had greater co-localisation of Gd-DTPA-BMA and Gadomer vessel leakiness (indicated in yellow) as seen in Fig. 3F.

Vasogenic oedema surrounding the solid tumour mass affected larger regions of the brain parenchyma in animals harbouring the rapidly growing U251-NG2 tumours than the more slowly growing U251-WT tumours at the initial scanning time-point, Fig. 3G, Mann–Whitney U test, $P = 0.040$. The vasogenic oedema was also more prominent in the U251-NG2 tumour bearing animals at the second time-point, Fig. 3H, Mann–Whitney U test, $P = 0.018$. When comparing the contribution of vasogenic oedema with the total lesion volume in animals with equivalent lesion volumes in the two groups (i.e. U251-NG2 at 5 weeks, and U251-WT at 7 weeks), peritumoural oedema contributed to 54% of the total affected brain region in the U251-NG2 tumour bearing animals and 30% in the U251-WT animals.

NG2 increases tumour growth

To study the effect of NG2 expression on tumour growth, human glioblastoma tumour spheroids derived from U251-WT (Fig. 4A) and U251-NG2 (Fig. 4D) tumour cells were implanted intracerebrally into immunodeficient nude rats and followed longitudinally using MRI. A histological comparison was done between the U251-WT (Fig. 4B) and the U251-NG2 tumours (Fig. 4E). The U251-WT tumours were highly cellular and homogeneous whereas the U251-NG2 tumours displayed numerous atypical cells with extensive areas of necrosis (Fig. 4E). Double labelling for NG2 with a pan-human anti-vimentin antibody confirmed the NG2 transgene expression in vivo by the human U251 tumour cells, Fig. 4F. In contrast, no NG2 expression was detected in the U251-WT tumours (data not shown). However, NG2 was expressed by oligodendrocyte precursor-like cells (Fig. 4C) in the normal brain.

Overexpression of NG2 in the glioblastoma cells accelerated both the development and growth of the U251-NG2 tumours compared to the U251-WT controls. All U251-NG2 tumour bearing animals developed visible tumours already at the first MRI time-point, with a mean solid tumour volume of 9 ± 4.4 mm^3 (mean ± SEM), Fig. 4G. In contrast, only four animals bearing the U251-WT tumours had MR visible tumours after 5 weeks, with a mean tumour volume of 2 ± 0.8 mm^3 (Fig. 4G). By the second scanning time-point, the U251-NG2 tumours had affected large regions of the hemisphere and caused a midline shift. The mean tumour volume in the NG2 group was 99.5 ± 38.2 mm^3 (Fig. 4H), with a mean tumour volume doubling time of 3.9 days. In contrast, estimation of the solid U251-WT tumour tissue revealed a significantly slower growth rate, with the mean tumour volume being 18.5 ± 8.9 mm^3 (Fig. 4H), Mann–Whitney U test, $P = 0.019$, and a mean tumour volume doubling time of 4.5 days. Four animals receiving the U251-NG2 tumours developed central

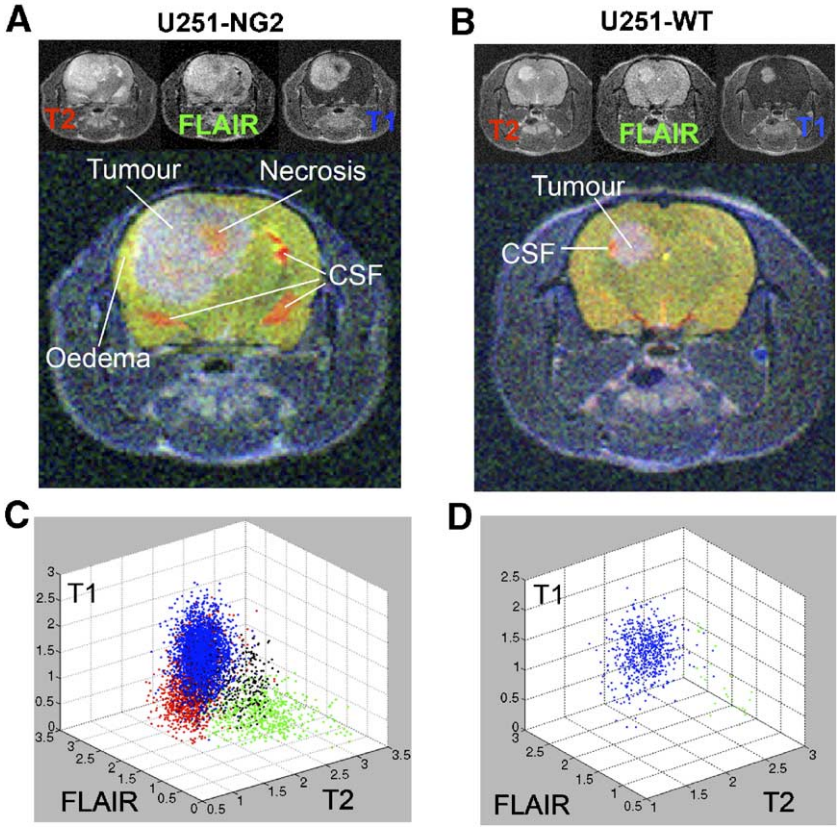

Fig. 5. Multispectral MRI imaging of tumour characteristics. Geometrically corresponding and co-registered T2-weighted (encoded red), FLAIR (encoded green) and T1-weigthed (encoded blue) images of (A) U251-NG2 and (B) U251-WT tumour bearing animal at the second time-point. The three-dimensional scatter plots, panels C and D, derived from the multispectral images show the combination of observed signal intensities in the three channels and represent the different features of the tumour. Points that are labelled blue represent pixels with solid tumour tissue, red points oedema, green points CSF, and black points necrotic tissue.

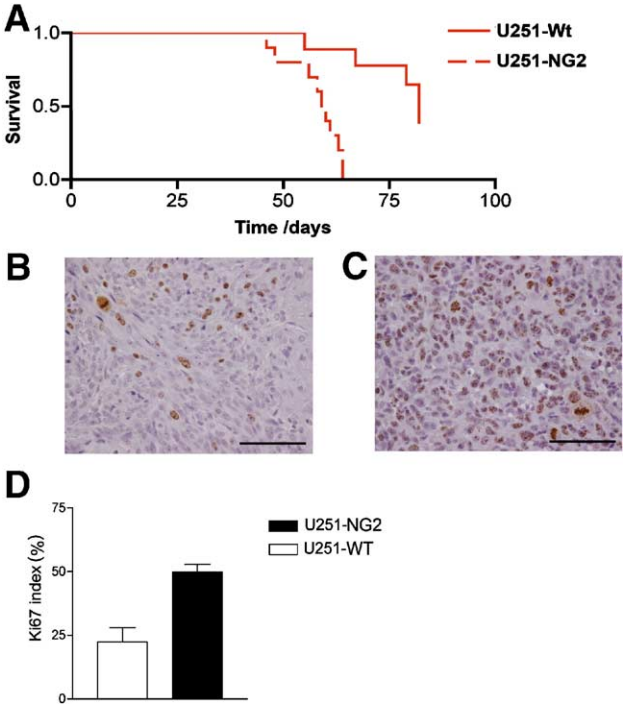

Fig. 6. NG2 expression in vivo predicts shorter survival outcomes. (A) Kaplan–Meier cumulative survival analyses for U251-NG2 and U251-WT recipient animals (n = 19 animals analysed), log rank$_{13.43}$; df = 1; P < 0.0002. Immunohistochemistry for Ki67 in (B) U251-WT (magnification 400×, scale bar 60 μm), and (C) U251-NG2 tumours (magnification 400×, scale bar 60 μm), showing proliferating tumour cells. (D) % Ki67 labelling index (mean ± SEM) in the U251-NG2 compared to the U251-WT tumours, unpaired Student's t test, $t_{4.31}$, df = 4, P = 0.0125. Quantified as described in Methods.

necrotic foci during the scanning periods whilst none of the U251-WT tumours depicted MRI visible necrotic regions at any of the two time-points, Fig. 4I. Multispectral MRI analyses of solid tumour tissue, oedema and necrosis were estimated by using the multichannel colour-encoding method, see Figs. 5A–D.

Furthermore, the U251-NG2 tumours were significantly more tumourigenic compared to the U251-WT tumours. All NG2-tumour bearing animals developed intracranial tumours (100%) compared to 5 out of 9 (55%) animals harbouring the U251-WT tumours. To investigate whether these effects of NG2 might expedite mortality, the survival outcomes for 19 animals were analysed. The animals receiving the U251-NG2 tumours (n = 10) had a significantly shorter survival, with a median survival of 59.5 days, compared with the control animals (n = 9), with a median survival of 82 days; log rank$_{13.43}$; df = 1; P < 0.0002, Fig. 6A. In line with these observations, Ki67 labelling confirmed that the NG2 positive tumours had a higher proliferative rate than their NG2 negative counterparts (Figs. 6B–D).

Discussion

The present study demonstrates that NG2 expressing tumour cells recruited host-derived neovasculature and regulated its morphology and function differently than the NG2 negative control tumours. These vascular changes coincided with a higher tumour take and a more rapid disease course suggesting that NG2 is a key regulator in the cross-talk between the tumour and its host microenvironment. Previously, we have shown that NG2 is expressed on both tumour cells and their associated vessels in biopsy tissue from glioma patients (Chekenya et al., 2002a), and that its expression increases with tumour grade. Thus, NG2 expression may provide a mechanism for stromal activation promoting tumour progression, leading towards a more aggressive disease course.

Consistent with previous studies (Chekenya et al., 2002b), histological analyses revealed that the U251-NG2 tumours were associated with increased microvessel density. However, using electron microscopy, we also found that the vascular elements had larger endothelial gaps, disrupted basement membranes and less pericyte coverage. Thus, NG2 not only mediates quantitative changes in the tumour vasculature, but also massive structural changes. Moreover, the functional implications were assessed using dynamic contrast-enhanced MRI that only measures perfused and functional vasculature. This technique provides a valuable supplement to MVD counts that do not distinguish between functional and non-functional vessels. The dynamic contrast-enhanced MRI analyses showed a higher blood supply and vessel permeability for high-molecular-weight contrast agents in the NG2 positive tumours. Therefore, our findings demonstrate that the U251-NG2 tumours are supplied by more functional vessels with bigger defects, as illustrated by the increased extravasation of Gadomer. This was also corroborated by large areas of intra-tumoural haemorrhage present in the tissue sections indicating increased vessel leakage (Liwnicz et al., 1987; Van den Brenk et al., 1977) that is associated with on-going angiogenesis and vascular remodelling (Hashizume et al., 2000).

Since U251-NG2 tumour bearing animals had a shorter survival, the increased permeability seen in this group might indicate a more aggressive and malignant phenotype. Several other groups have also reported a correlation between vessel leakiness and pathological grade using dynamic contrast-enhanced MRI in animal models (van Dijke et al., 1996) and in humans (Daldrup et al., 1998; Gossmann et al., 2000; Roberts et al., 2000).

In contrast, Gd-DTPA-BMA enhanced more homogeneously in both tumours, due to a more rapid leakage and diffusion of the smaller particles. Thus, high- or intermediate-molecular-weight contrast agents may provide a more reliable estimate of the fractional blood volume and differences in permeability between tumours (Buckley et al., 2004). Our findings are in this respect consistent with reports from other studies (Roberts, 1997; Su et al., 1999). Furthermore, since the biodistribution of a drug within the tumour bed depends on microvascular perfusion, permeability and diffusion (Jain, 1989), the distribution studies of Gadomer in solid tumour tissue may predict the efficacy of a given therapeutic agent. Gd-DTPA-BMA on the other hand, seems more suitable for the delineation and visualisation of the viable tumour tissue.

The elimination rate of Gadomer from the tissue in the U251-NG2 was not distinguishable from that of the U251-WT tumours at 7 weeks. U251-NG2 tumours showed a decrease in wash-out rate of tracer from 5 to 7 weeks within the NG2 positive tumour group. Contrast media elimination from necrotic tissue is relatively slow (Matsubayashi et al., 2000) and may explain this finding, since histological and multispectral MRI analyses both revealed that large necrotic regions had developed in these tumours by the 7th week.

Although the U251-NG2 tumours were highly vascularised, their structurally irregular, large and frequently collapsing thin-

walled vessels are most likely due to an inability to match the rapid growth of the neoplastic cells. Although T1-weighted imaging with Gd-DTPA-BMA is used clinically for the detection of necrosis and delineation from viable tumour, the lack of enhancement does not always indicate necrosis. Therefore, we combined post-Gd-DTPA-BMA T1-weighted, T2-weighted and FLAIR sequences to limit the risk of false positive necrosis. Multisequence imaging and analyses of necrotic areas using colour encoded images correlated well with the tissue histology, and were also effective in visualising and distinguishing other fundamental tumour features such as oedema and entrapment of CSF. The U251-NG2 tumour bearing animals developed a more extensive vasogenic oedema in the surrounding brain parenchyma than animals with NG2 negative tumours, which may be explained by a disruption of the blood–brain barrier seen in the NG2 tumours. In addition, recent studies have shown that NG2 accelerates u-PA-dependent proteolysis of plasminogen to plasmin (Goretzki et al., 2000) that is involved in the degradation of the ECM and basement membranes. The break-down of these structures is accompanied by the sequestering of fluid into the interstitial tissue (Davies, 2002), which may further contribute to the vasogenic oedema.

Multisequence imaging and multispectral analysis proved to be a powerful tool in characterising the tumour phenotypes. However, when acquiring a high number of sequences, there is trade-off between acquisition time and image quality. The spatial resolution of DCE images was not ideal (i.e. 0.47 × 0.47 × 3 mm), but increasing the spatial resolution would affect the temporal resolution of the dynamic sequence using the imaging system available for this study. Moreover, increased spatial resolution would further increase the total imaging time (here 70 min), which we wanted to minimise in order to ensure that the animals survived the scanning sessions. Although, the temporal resolution of the dynamic contrast-enhanced imaging was 16.7 s in the first 30 frames where leakage of Gadomer from vessels to tumour tissue dominated, the transfer of the contrast agent is dependent on both diffusion and convection. These processes are relatively slow compared to the blood flow. Furthermore, the microvascular parameters were estimated by Gauss–Newton non-linear least-squares data fitting on a pixel-by-pixel basis. Since this showed a good line fit, it would indicate that our temporal resolution was sufficient. Moreover, the temporal resolution used in this study is in keeping with other permeability studies of small animals (Verhoye et al., 2002; Su et al., 1998).

Gd-DTPA-BMA was injected approximately 40 min after injection of Gadomer. Visual inspection of images acquired towards the end of the dynamic sequence showed wash-out of Gadomer from tumour tissue. Further post-processing of the images, by measurement of SI and tracer concentration over time, revealed that the signal intensity had almost reached the baseline values in most regions of the tumour, where a very low tissue concentration was found. The influence of Gadomer on the SI in the SE T1-weighted and on the distribution of Gd-DTPA-BMA was therefore negligible, ruling out possible interference of Gadomer on the SI in the SE T1-weighted image and tissue distribution of Gd-DTPA-BMA. Furthermore, since it was critical to minimise the time elapsed between the sequences in order to avoid animal mortality due to prolonged general anaesthesia, the wash-out of Gadomer was not empirically confirmed by a pre-Gd-DTPA-BMA SE T1-weigted sequence.

We observed a 55% tumour take in the control group, compared to 100% in the U251-NG2 tumours, which also showed higher proliferative rate as indicated by higher Ki67 labelling indices and shorter in vivo tumour volume doubling times. These results correlate well with previous findings that demonstrated that NG2 expression increased the proliferation of melanoma and glioma cells in vitro and their tumourigenicity and metastatic potential in vivo (Burg et al., 1998; Chekenya et al., 1999, 2002b). The increased tumourigenicity is likely due to induction of tumour angiogenesis. Indeed, recent studies show that proteolytically cleaved and soluble forms of the NG2 proteoglycan induce endothelial cell migration, promote the assembly of capillary networks and stimulate angiogenesis in vivo by binding to galectin-3 and $\alpha 3\beta 1$ integrin receptors on endothelial cells (Fukushi et al., 2004). It has also been previously reported that NG2 interacts with angiostatin and neutralises the latter's ability to inhibit endothelial cell proliferation (Goretzki et al., 2000), emphasising the role for NG2 in promoting angiogenesis through pericyte-endothelial cell cross-talk in the host microenvironment.

Since NG2 is expressed on the cell surface, its involvement in tumour–host interactions makes it an attractive candidate for targeted therapies. Because NG2 regulates the transition from small, poorly vascularised tumours to large, highly vascular and aggressive tumours, we and others postulate that it may be an amenable therapeutic target (Chekenya and Pilkington, 2002; Grako et al., 1999; Ozerdem, 2004; Ozerdem and Stallcup, 2004; Winkler et al., 2004).

The fact that NG2 is present on the tumour cells as well as on the host-derived neovasculature, would also allow for simultaneously targeting both the malignant and stromal cell compartments within the tumour. Since stromal cells are non-transformed, they are less likely to develop drug resistance, which is a leading cause of treatment failure. Finally, our findings demonstrate that dynamic contrast-enhanced MRI is a valuable and reliable tool to study functional vascular dynamics in brain tumours non-invasively in vivo. DCE is so far the imaging technique for evaluating tumours clinically with respect to their state of functional microcirculation, as positron emission tomography is better at resolving larger vessel structures (Padhani, 2002). Two different pharmacokinetic models both confirmed the differences in permeability between the two groups, ruling out that our findings were model-dependent and making our findings more robust. The spatial pattern of contrast enhancement with Gadomer in solid tumour tissue might indicate the biodistribution of blood-bourne molecules used in therapeutic strategies, and thus is useful for treatment planning. In addition, serial multispectral MRI may give valuable information about other fundamental tumour features such as the development and progression of necrosis or oedema, which may be prognostically relevant.

Acknowledgments

The authors thank Schering AG and Dr. Berndt Misselwitz for providing Gadomer. We are grateful to Trond E. Singstad for technical assistance during the MR scanning and Eli Renate Grüner for computing decay rates of Gadomer in rat blood. We are also grateful to Bodil Hansen and Tove Johannsen for EM technical assistance. This study was supported by research grants from the Norwegian Research Council, the University of Bergen, Norway, the Norwegian Cancer Society and Helse-Vest, Haukeland University Hospital, Norway.

References

Buckley, D.L., Roberts, C., Parker, G.J., Logue, J.P., Hutchinson, C.E., 2004. Prostate cancer: evaluation of vascular characteristics with dynamic contrast-enhanced T1-weighted MR imaging—Initial experience. Radiology 233 (3), 709–715.

Burg, M.A., Grako, K.A., Stallcup, W.B., 1998. Expression of the NG2 proteoglycan enhances the growth and metastatic properties of melanoma cells. J. Cell. Physiol. 177 (2), 299–312.

Burger, P.C., Kleihues, P., 1989. Cytologic composition of the untreated glioblastoma with implications for evaluation of needle biopsies. Cancer 63 (10), 2014–2023.

Chekenya, M., Pilkington, G.J., 2002. NG2 precursor cells in neoplasia: functional, histogenesis and therapeutic implications for malignant brain tumours. J. Neurocytol. 31 (6–7), 507–521.

Chekenya, M., Rooprai, H.K., Davies, D., Levine, J.M., Butt, A.M., Pilkington, G.J., 1999b. The NG2 chondroitin sulfate proteoglycan: role in malignant progression of human brain tumours. Int. J. Dev. Neurosci. 17 (5–6), 421–435.

Chekenya, M., Enger, P.O., Thorsen, F., Tysnes, B.B., Al-Sarraj, S., Read, T.A., Furmanek, T., Mahesparan, R., Levine, J.M., Butt, A.M., Pilkington, G.J., Bjerkvig, R., 2002a. The glial precursor proteoglycan, NG2, is expressed on tumour neovasculature by vascular pericytes in human malignant brain tumours. Neuropathol. Appl. Neurobiol. 28 (5), 367–380.

Chekenya, M., Hjelstuen, M., Enger, P.O., Thorsen, F., Jacob, A.L., Probst, B., Haraldseth, O., Pilkington, G., Butt, A., Levine, J.M., Bjerkvig, R., 2002b. NG2 proteoglycan promotes angiogenesis-dependent tumor growth in CNS by sequestering angiostatin. FASEB J. 16 (6), 586–588.

Daldrup, H., Shames, D.M., Wendland, M., Okuhata, Y., Link, T.M., Rosenau, W., Lu, Y., Brasch, R.C., 1998. Correlation of dynamic contrast-enhanced MR imaging with histologic tumor grade: comparison of macromolecular and small-molecular contrast media. AJR Am. J. Roentgenol. 171 (4), 941–949.

Davies, D.C., 2002. Blood–brain barrier breakdown in septic encephalopathy and brain tumours. J. Anat. 200 (6), 639–646.

Donahue, K.M., Weisskoff, R.M., Burstein, D., 1997. Water diffusion and exchange as they influence contrast enhancement. J. Magn. Reson. Imaging 7 (1), 102–110.

Folkman, J., 1995. Angiogenesis in cancer, vascular, rheumatoid and other disease. Nat. Med. 1 (1), 27–31.

Folkman, J., Merler, E., Abernathy, C., Williams, G., 1971. Isolation of a tumor factor responsible for angiogenesis. J. Exp. Med. 133 (2), 275–288.

Fukushi, J., Makagiansar, I.T., Stallcup, W.B., 2004. NG2 proteoglycan promotes endothelial cell motility and angiogenesis via engagement of galectin-3 and alpha3beta1 integrin. Mol. Biol. Cell 15 (8), 3580–3590.

Goretzki, L., Lombardo, C.R., Stallcup, W.B., 2000. Binding of the NG2 proteoglycan to kringle domains modulates the functional properties of angiostatin and plasmin(ogen). J. Biol. Chem. 275 (37), 28625–28633.

Gossmann, A., Helbich, T.H., Mesiano, S., Shames, D.M., Wendland, M.F., Roberts, T.P., Ferrara, N., Jaffe, R.B., Brasch, R.C., 2000. Magnetic resonance imaging in an experimental model of human ovarian cancer demonstrating altered microvascular permeability after inhibition of vascular endothelial growth factor. Am. J. Obstet. Gynecol. 183 (4), 956–963.

Grako, K.A., Ochiya, T., Barritt, D., Nishiyama, A., Stallcup, W.B., 1999. PDGF (alpha)-receptor is unresponsive to PDGF-AA in aortic smooth muscle cells from the NG2 knockout mouse. J. Cell. Sci. 112 (Pt 6), 905–915.

Hashizume, H., Baluk, P., Morikawa, S., McLean, J.W., Thurston, G., Roberge, S., Jain, R.K., McDonald, D.M., 2000. Openings between defective endothelial cells explain tumor vessel leakiness. Am. J. Pathol. 156 (4), 1363–1380.

Holash, J., Maisonpierre, P.C., Compton, D., Boland, P., Alexander, C.R., Zagzag, D., Yancopoulos, G.D., Wiegand, S.J., 1999. Vessel cooption, regression, and growth in tumors mediated by angiopoietins and VEGF. Science 284 (5422), 1994–1998.

Jain, R.K., 1989. Delivery of novel therapeutic agents in tumors: physiological barriers and strategies. J. Natl. Cancer Inst. 81 (8), 570–576.

Kaplan, I.W., Meier, R., 1959. Submucous lipoma of the colon. Am. J. Gastroenterol. 31 (6), 673–683.

Klagsbrun, M., Knighton, D., Folkman, J., 1976. Tumor angiogenesis activity in cells grown in tissue culture. Cancer Res. 36 (1), 110–114.

Liwnicz, B.H., Wu, S.Z., Tew Jr., J.M., 1987. The relationship between the capillary structure and hemorrhage in gliomas. J. Neurosurg. 66 (4), 536–541.

Mantel, N., Haenszel, W., 1959. Statistical aspects of the analysis of data from retrospective studies of disease. J. Natl. Cancer Inst. 22 (4), 719–748.

Matsubayashi, R., Matsuo, Y., Edakuni, G., Satoh, T., Tokunaga, O., Kudo, S., 2000. Breast masses with peripheral rim enhancement on dynamic contrast-enhanced MR images: correlation of MR findings with histologic features and expression of growth factors. Radiology 217 (3), 841–848.

McDonald, D.M., Choyke, P.L., 2003. Imaging of angiogenesis: from microscope to clinic. Nat. Med. 9 (6), 713–725.

Misselwitz, B., Schmitt-Willich, H., Ebert, W., Frenzel, T., Weinmann, H.J., 2001. Pharmacokinetics of Gadomer-17, a new dendritic magnetic resonance contrast agent. Magma 12 (2–3), 128–134.

Nakajima, M., Nakasu, S., Morikawa, S., Inubushi, T., 1998. Estimation of volume doubling time and cell loss in an experimental rat glioma model in vivo. Acta Neurochir. (Wien) 140 (6), 607–612 (discussion 612–613).

Nehls, V., Denzer, K., Drenckhahn, D., 1992. Pericyte involvement in capillary sprouting during angiogenesis in situ. Cell Tissue Res. 270 (3), 469–474.

Ozerdem, U., 2004. Targeting neovascular pericytes in neurofibromatosis type 1. Angiogenesis 7 (4), 307–311.

Ozerdem, U., Stallcup, W.B., 2003. Early contribution of pericytes to angiogenic sprouting and tube formation. Angiogenesis 6 (3), 241–249.

Ozerdem, U., Stallcup, W.B., 2004. Pathological angiogenesis is reduced by targeting pericytes via the NG2 proteoglycan. Angiogenesis 7 (3), 269–276.

Ozerdem, U., Grako, K.A., Dahlin-Huppe, K., Monosov, E., Stallcup, W.B., 2001. NG2 proteoglycan is expressed exclusively by mural cells during vascular morphogenesis. Dev. Dyn. 222 (2), 218–227.

Ozerdem, U., Charbono, W.L., Stallcup, W.B., 2002. Plastic casting of embryonic, placental, and tumor vasculature in the mouse. Microvasc. Res. 64 (3), 486–490.

Padhani, A.R., 2002. Dynamic contrast-enhanced MRI in clinical oncology: current status and future directions. J. Magn. Reson. Imaging 16 (4), 407–422.

Roberts, T.P., 1997. Physiologic measurements by contrast-enhanced MR imaging: expectations and limitations. J. Magn. Reson. Imaging 7 (1), 82–90.

Roberts, H.C., Roberts, T.P., Brasch, R.C., Dillon, W.P., 2000. Quantitative measurement of microvascular permeability in human brain tumors achieved using dynamic contrast-enhanced MR imaging: correlation with histologic grade. AJNR Am. J. Neuroradiol. 21 (5), 891–899.

Sang, U.H., Kelley, P.Y., Hatton, J.D., Shew, J.Y., 1989. Proto-oncogene abnormalities and their relationship to tumorigenicity in some human glioblastomas. J. Neurosurg. 71 (1), 83–90.

Schlingemann, R.O., Rietveld, F.J., de Waal, R.M., Ferrone, S., Ruiter, D.J., 1990. Expression of the high molecular weight melanoma-associated antigen by pericytes during angiogenesis in tumors and in healing wounds. Am. J. Pathol. 136 (6), 1393–1405.

Su, M.Y., Jao, J.C., Nalcioglu, O., 1994. Measurement of vascular volume fraction and blood–tissue permeability constants with a pharmacokinetic model: studies in rat muscle tumors with dynamic Gd-DTPA enhanced MRI. Magn. Reson. Med. 32 (6), 714–724.

Su, M.Y., Muhler, A., Lao, X., Nalcioglu, O., 1998. Tumor characterization with dynamic contrast-enhanced MRI using MR contrast agents of various molecular weights. Magn. Reson. Med. 39 (2), 259–269.

Su, M.Y., Wang, Z., Nalcioglu, O., 1999. Investigation of longitudinal vascular changes in control and chemotherapy-treated tumors to serve as therapeutic efficacy predictors. J. Magn. Reson. Imaging 9 (1), 128–137.

Thorsen, F., Ersland, L., Nordli, H., Enger, P.O., Huszthy, P.C., Lundervold, A., Standnes, T., Bjerkvig, R., Lund-Johansen, M., 2003. Imaging of experimental rat gliomas using a clinical MR scanner. J. Neuro-oncol. 63 (3), 225–231.

Tofts, P.S., 1997. Modeling tracer kinetics in dynamic Gd-DTPA MR imaging. J. Magn. Reson. Imaging 7 (1), 91–101.

Tofts, P.S., Kermode, A.G., 1991. Measurement of the blood–brain barrier permeability and leakage space using dynamic MR imaging: 1. Fundamental concepts. Magn. Reson. Med. 17 (2), 357–367.

Tofts, P.S., Brix, G., Buckley, D.L., Evelhoch, J.L., Henderson, E., Knopp, M.V., Larsson, H.B., Lee, T.Y., Mayr, N.A., Parker, G.J., Port, R.E., Taylor, J., Weisskoff, R.M., 1999. Estimating kinetic parameters from dynamic contrast-enhanced T(1)-weighted MRI of a diffusable tracer: standardized quantities and symbols. J. Magn. Reson. Imaging 10 (3), 223–232.

Van den Brenk, H.A., Crowe, M., Kelly, H., Stone, M.G., 1977. The significance of free blood in liquid and solid tumours. Br. J. Exp. Pathol. 58 (2), 147–159.

van Dijke, C.F., Brasch, R.C., Roberts, T.P., Weidner, N., Mathur, A., Shames, D.M., Mann, J.S., Demsar, F., Lang, P., Schwickert, H.C., 1996. Mammary carcinoma model: correlation of macromolecular contrast-enhanced MR imaging characterizations of tumor microvasculature and histologic capillary density. Radiology 198 (3), 813–818.

Verhoye, M., Van der Sanden, B.P., Rijken, P.F., Peters, Hp., Van der Kogel, A.J., Pee, G., Vanhoutte, G., Hearschap, A., Van der Linden, A., 2002. Assessment of the neovascular permeability in glioma xenografts by Dynamic T(1) MRI with Gadomer 17. Magn. Reson. Med. 47 (2), 305–313.

Winkler, F., Kozin, S.V., Tong, R.T., Chae, S.S., Booth, M.F., Garkavtsev, I., Xu, L., Hicklin, D.J., Fukumura, D., di Tomaso, E., Munn, L.L., Jain, R.K., 2004. Kinetics of vascular normalization by VEGFR2 blockade governs brain tumor response to radiation: role of oxygenation, angiopoietin-1, and matrix metalloproteinases. Cancer Cells 6 (6), 553–563.

Yuhas, J.M., Li, A.P., Martinez, A.O., Ladman, A.J., 1977. A simplified method for production and growth of multicellular tumor spheroids. Cancer Res. 37 (10), 3639–3643.